Insights into highly effective catalytic persulfate activation on oxygen-functionalized mesoporous carbon for Ciprofloxacin degradation

ying xiong
Changsha University of Science and Technology
Xiaolei Dai
Changsha University of Science and Technology - Yuntang Campus: Changsha University of Science and Technology
Yuanyuan Liu (lyy8838@126.com)
Changsha University of Science and Technology https://orcid.org/0000-0003-4242-1252
Chunyan Du
Changsha University of Science and Technology - Yuntang Campus: Changsha University of Science and Technology
Guanlong Yu
Changsha University of Science and Technology - Yuntang Campus: Changsha University of Science and Technology
Yan Xia
Changsha University of Science and Technology - Yuntang Campus: Changsha University of Science and Technology

Research Article

Keywords: Persulfate, Advanced oxidation processes, Oxygen-functionalized mesoporous carbon, Ciprofloxacin, Radical and nonradical

Posted Date: January 25th, 2022

DOI: https://doi.org/10.21203/rs.3.rs-945390/v1

Version of Record: A version of this preprint was published at Environmental Science and Pollution Research on April 5th, 2022. See the published version at https://doi.org/10.1007/s11356-022-19670-5.

Abstract

Nanocarbons have been demonstrated as promising carbon catalysts for substituting metal-based catalysts for the green treatment of wastewater. In this study, oxygen-functionalized mesoporous carbon (OCMK-3) was prepared by wet oxidation and exhibited high catalytic performance against ciprofloxacin (CIP) by activation of persulfate. The effects of environmental parameters (pH, temperature, coexisting ions) and process parameters (temperature, sodium persulfate concentration, catalyst agent dosage, initial concentration) on the removal of CIP were investigated. Compared with the pristine ordered mesoporous carbon (CMK-3), the removal efficiency of CIP by OCMK-3 was increased by 32% under optimal conditions. This rise in activity was attributed to the increase in oxygen-containing functional groups, porosity and specific surface area of OCMK-3 with improved structural defects and electron transfer efficiency. Furthermore, based on active species scavenging experiments, a dual-pathway mechanism of the radical and nonradical pathways was discovered. The rational degradation pathway of CIP was investigated based on liquid chromatography-mass spectrometry (LC-MS). In addition, the OCMK-3/PS system exhibited high decomposition efficiency in pharmaceutical wastewater treatment. This study provides an in-depth mechanism for the degradation of organic pollutants by carbon-based PS-AOPs and provides theoretical support for further studies.

1. Introduction

Pharmaceuticals, mainly antibiotics, are emerging contaminants that are frequently found in the environment worldwide through continuous discharge from sewage pipes and environmental accumulation. (Liu and Jin et al., 2015; Meena and Dotaniya et al., 2015). The presence of antibiotics, even at low concentrations, could pose severe threats to the ecosystem and human health mainly through antibacterial resistance and possible toxicity. However, the chemical complexity and diversity make antibiotics difficult to remove in conventional wastewater treatment plants.(Tello and Austin et al., 2012; Su and Pan et al., 2014). Therefore, in order to remove antibiotics from water bodies, several techniques such as advanced oxidation processes (AOP) (Anjali and Shanthakumar, 2019; Cuerda-Correa and Alexandre-Franco et al., 2019; Wang and Zhuan, 2019; Du and Zhang et al., 2021), adsorption(Torres-Perez and Gerente et al., 2012; Li and Di et al., 2014) and biodegradation(Mueller and Schuessler et al., 2013; Fonseca and De, 2020) have been extensively researched. Among them, AOP technology is considered to be one of the most effective ways for antibiotic removal due to the reaction with reactive radicals, including sulfate and hydroxyl radicals (·OH and $SO_4{\cdot}^-$) (Li and Zhou et al., 2017; Thanekar and Panda et al., 2018). Compared with traditional AOP based on ·OH, novel AOP based on sulfate radicals (SR-AOPs) has been extensively applied in water treatment, as peroxymonosulfate (PMS) or persulfate (PS) using in SR-AOPs are more stable, easier to store and cheaper than liquid H_2O_2. Besides, $SO_4{\cdot}^-$ possess higher standard oxidation potential and longer lifetime than ·OH(Yang and Chen et al., 2008; Furman and Teel et al., 2010; Mushtaque and Ahmad et al., 2013; Duan and Xiaoguang et al., 2018), therefore draw increasing attention.

PS could be activated using many methods, such as illumination, heat activation, ultrasonicl activation, microwave activation, metal-based material activation and metal-free catalyst activation(Matzek and Carter, 2016; Shao and Duan et al., 2017). Compared with homogeneous activation system which requires intensive energy inputs or high dosages of chemical impost, heterogeneous systems based on transitional metals/metal oxides and carbonaceous materials have been widely investigated. In contrast with metal-based heterogeneous systems, carbonaceous materials could avoid secondary contamination by metals, heat or alkalinity, exhibit high efficiency and stability, in line with the development strategy of green remediation(Hao and Carroll, 2016; Guo and Zeng et al., 2017). Among metal-free carbonaceous catalysts, ordered mesoporous carbon is of great interest because of its regular spherical morphology, abundant mesopores, large specific surface area, high chemical stability and good electrical conductivity(Zhu and Wang et al., 2015; Du and Zhang et al., 2020).

Previous studies have shown that catalytic materials play a synergistic role in specific applications due to their surface chemistry and pore structure. Both surface chemistry and pore structure modifications have been demonstrated to improve the performance of catalysts(Xu and Farber et al., 2003; Bazu A and Lu et al., 2008). To increase active sites of the catalysts and thus enhance the catalytic performance, carbonaceous materials are usually post-treated by oxidation, polymer coating, grafting, etc.(Gómez-Serrano and Piriz-Almeida et al., 1999; Kim and Kang et al., 2011; Vara and Collazos-Castro, 2019). Among these modification methods, surface oxidation is one of the most convenient and commonly used methods. The oxygen-containing groups could be introduced into the surface of the catalysts through surface oxidation, which might offer more active sites for persulfate activation, and the hydrophilicity of the surface could also get improved (Bazu A and Lu et al., 2008), making the catalysts more suitable for further applications. Although there have been some studies about oxygen-functionalized mesoporous carbon (OCMK-3), very few of them reported activating PS using OCMK-3.

Therefore, to reveal the mechanism involved in OMCK-3 based SR-AOPs for the removal of aqueous organic pollutants, the commonly used antibiotic ciprofloxacin (CIP) was selected as the target pollutant. The removal of CIP in OMCK-3/PS system under different conditions was studied. Considering the superior adsorption performance of OCMK-3, the relationship between adsorption and catalytic processes was discussed. The reaction mechanism of the OCMK-3/PS system was discussed based on the experimental results of free radical burst, electron paramagnetic resonance (EPR), and liquid chromatography-mass spectrometry (LC-MS). The application prospects of the OCMK-3/PS system were also evaluated using real pharmaceutical wastewater samples.

2. Materials And Methods

2.1. Chemicals

Ciprofloxacin (CIP) was purchased from Macklin, sodium peroxydisulfate (PS, $Na_2S_2O_8$), methanol (MeOH), Ethanol (EtOH), 1,4-benzoquinone (BQ), were purchased from Sinopharm Chemical Regent Co. Ltd. (Shanghai, China). Pluronic copolymer P123 ($EO_{20}PO_{70}EO_{20}$) (Mav = 5800), tetraethyl orthosilicate

(TEOS) ($SiC_8H_{20}O4$, 98%) are purchased from Sigma–Aldrich (USA). All chemicals were at least chemical grade and were used as received without further puri□cation.

2.2. Preparation of CMK-3/OCMK-3

At first, hexagonal mesoporous silica (SBA-15) was synthesized according to the typical method as reported. SBA-15 was used as a hard template to prepare mesoporous carbon (CMK-3) (Jun, 2000). The details of the synthesis procedures of SBA-15 and CMK-3 were provided in Supporting Information (SI).

CMK-3 was oxidized by wet oxidation at different nitric acid concentrations, contact temperatures and oxidation time. Typically, 0.1 g of dried CMK-3 powder was treated with 15 ml of HNO_3 solution (1, 2, 4, 6 M solution) under refluxing for 15 min to 60 min at a temperature range of 70-90°C to prepare OCMK-3. After oxidation, mesoporous catalysts were filtered and washed with ultrapure water until solution was neutral(Nejad and Shams et al., 2016). OCK-3 synthesized under optimal conditions were then used for characterization and the removal of CIP.

2.3. Materials characterization

The morphological information of the two catalysts was obtained employing transmission electron microscopy (TEM, JEOL-1230). The nitrogen adsorption/desorption isotherm was obtained using Brunauer-Emmett-Teller (BET) method with a Micromeritics ASAP 2020, and the pore size properties of the materials were derived from the adsorption branches of isotherm using the BJH (Barret-Joyner-Halenda) method. To characterize the functional groups within the CMK-3 and OCMK-3 catalysts, Fourier-transform infrared spectroscopy (FTIR) on a PerkinElmer instrument (Spectrum GX, USA) within the 400–4000 cm^{-1} region was employed. The surface chemistry and chemical states of elements before and after the reaction were investigated, using X-ray photoelectron spectroscopy (XPS) by a Thermo ESCALAB 250XI instrument under an Al-Kα X-ray radiation. Zeta Potential was determined by dispersing CMK-3 and OCMK-3 in 1 mmol/L NaCl solution with various pH values through ultrasonic treatment, and then measuring the supernatant with Zetasizer Nano (ZEN3600, Malvern).

2.4. Catalytic activity tests

Batch experiments were conducted in 100ml conical flasks in a thermostatic shaker, with the shaking rate at 150 rpm and temperature maintained at 25 ℃. Typically, OCMK-3 was first added to a series of conical flasks containing 50 mL of 200 mg/L CIP solution (pH 5 without any buffering). After shaking for 1 h to reach adsorption-desorption equilibrium, a certain amount of PS was added to activate the catalytic process and shaken for another 2 h. Generally, unless otherwise mentioned, 0.2 g/L of OCMK-3 and 8 mM of PS were used in the system, and. 0.1 M HNO_3 or NaOH were used to adjust the solution pH. The mixed solution was taken at each time interval, filtered and then added to a centrifuge tube containing 1ml of methanol, which was employed to scavenge the active free radicals and quench the further oxidation reaction. The experiment procedure for pharmaceutical wastewater sample was conducted the same as above.

As a relatively crucial index for catalysts, after the completion of the experimental system reaction, OCMK-3 was recycled by ethanol and water, dried at 60 ℃ and reused for three cycles. To study the roles of active free radicals, certain amounts of radical scavengers were added into the system. MeOH, EtOH and 1,4-benzoquinone (BQ) were used (calibrated by molar ratio MeOH/PS, EtOH /PS or BQ/PS) to scavenge $SO_4 \cdot^-$, ·OH and $O_2 \cdot^-$, respectively. Experimental samples were conducted in triplicate, with the average values reported as the results.

2.4. Analytical methods

The concentration of CIP wasmeasured by the UV2600 ultraviolet spectrophotometer at wavelengths 275.5 nm(Tran and Nguyen et al., 2019). The generated active radicals, $SO_4 \bullet^-$, •OH and O_2^-, were detected on a Bruker ER200-SRC spectrometer using 5,5-dimethyl-1-pyrroline N-oxide (DMPO) as spin-trapping agent. Thepharmaceutical wastewater samples were analyzed usingthree-dimensional excitation-emission matrix (3D-EEM) fluorescence spectroscopy with the excitation wavelengths ranging from 200 nm to 600 nm, and the emission wavelengths ranging from 200 nm to 900 nm. The intermediateproducts of CIP after OCMK-3/PS treatment were identified by LC/MS.

2.5. Pharmaceutical wastewater sample treatment

In order to test the practical potential, the OCMK-3 was applied in the treatment of pharmaceutical wastewater, which was gathered from Liu yang Bio-medicine Garden (Hunan province, China). The sample was brownish-yellow in color and had strong pungent smell. The contents in the wastewater mainly contained alcohols, bufexamac, 1-bromobutane, hydroxylamine and other organic matters.

3. Results And Discussion

3.1. Characterization

TEM was used to observe the morphology of CMK-3 and OCMK-3, with the results shown in Fig. 1. The well-ordered stripe-like structures could be clearly observed from Fig. 1(a) and (b), indicating that oxidation did not destroy the ordered mesoporous structure of CMK-3. The isotherm curve of both catalysts (inset of Fig. 2) exhibited type IV feature, indicating the typical mesoporous structures. Based on the pore size distributions curves (Fig. 2), the most probable pore sizes of the two materials centered around 5 nm, indicating the uniform mesopores of them, in agreement with the TEM images(Wang and Man et al., 2018). Meanwhile, the specific pore structure parameters of both catalysts are listed in Table S3.

The changes of CMK-3 and OCMK-3 in the composition of functional groups before and after reaction were analyzed using XPS. As shown in the wide scan XPS spectra (Fig. 3(a, b)), The oxygen content of OCMK-3 was higher than that of CMK-3 before and after reaction, indicating that more oxygen-containg groups were introduced after the oxidation treatment, and resulted in the improvement of the catalytic effect. Meanwhile, both CMK-3 and OCMK-3 spectra showed the increased oxygen level after reaction

owing to intermediates adsorption and the surface oxidation, which was consistent with the previous studies(Duan and Su et al., 2016). Fig. 3(c-f) shows the de-convolution XPS C1s and O1s spectra before and after the reaction. Before reaction, high solution C1s XPS spectra of CMK-3 could be divided into three sections corresponding to t C graphite/C-C/C-H (283.85 eV), C-OH/C-O-C (284.77 eV) and π-π* (287.94 eV) shake up, respectively. After reaction, a broad C1s peak of CMK-3 was fitted into four component peaks at 284.34, 285.92, 287.12 and 288.42 eV, indicating C graphite/C-C/C-H, C=O, COOH and π-π* shake up. Meanwhile, before reaction, C1s XPS spectra represented three C species on original OCMK-3 in the range of 282–292 eV: C graphite/C-C/C-H, C-OH/C-O-C and π-π* shake up generated at 283.58, 284.77 and 287.77 eV, respectively. After reaction, a broad C1s peak was fitted into four C species on OCMK-3 in the range of 282–292 eV: C graphite/C-C/C-H, C=O, COOH and π-π* shake up generated at 284.34, 285.92 and 287.12 eV, 288.42eV, respectively. After reaction, the C-OH/C-O-C on the surface of both CMK-3 and OCMK-3 decreased, and C=O and COOH increased. Therefore, it could be conferred that in the process of PS activation by the two materials, the hydroxyl groups on the surface were converted into carbonyl and carboxyl groups. Thus hydroxyl on the surface could be regarded as an important functional group for catalysts activation. As shown in Fig. 3(d, f), high solution O1s XPS spectra could be divided into three types of O species: O1(530.98–531.9 eV), O2(532.6–533.6 eV), and O3 (533.5–535.84 eV) indicating C=O, C-OH/C-O-C and chemisorbed oxygen and adsorbed water, respectively. For the speci□c oxygen groups, both C1s and O1s scans displayed the increase of C-OH/C-O-C and the decrease of C=O after reaction, which might be ascribed to the transformation between the two groups. Therefore, the changes of the speci□c groups might impose effects on the catalytic performances of the catalysts(Indrawirawan and Sun et al., 2015; Tang and Liu et al., 2018). The influence of trace amounts of nitrogen on the surface of the catalyst was also investigated. The de-convolution XPS N1s spectra of CMK-3 and OCMK-3 before reaction were shown in Fig. S1(a-b). Obviously, after oxidation of CMK-3 using nitric acid, nitrogen-containing functional groups were introduced on the surface. The N1s peak of OCMK-3 was fitted into two sections at 399 and 405 eV, indicating pyridine and $-NO_2$. It was also conferred in other studies that under a high temperature environment, oxidation using HNO_3 could effectively generate nitrogen-containing species on the surface(Yang and Li et al., 2016).

FT-IR spectroscopy (Fig. 4) was also used for further studies of the surface chemistry of CMK-3 and OCMK-3. The absorption of stretching vibration of C–O bond was denoted in the absorption band at 1100 cm^{-1}. Peak around 1640 cm^{-1} corresponded to C=O and -OH stretch vibrations and the characteristic peaks around 2922 $cm^{-1}$and 3440 cm^{-1} indicated C-H/O-H and -OH stretch vibrations, respectively. The relative intensity of 1100 cm^{-1}, 1640 cm^{-1} and 2922 cm^{-1} bands in OCMK-3 were higher than those of the CMK-3 sample, indicating that more C–O,C=O, –OH and C-H/O-H functional groups were generated after the oxidation(Zolfaghari and Esmaili-Sari et al., 2011). Therefore, FT-IR spectra further demonstrated the presence of more oxygen-containing functional groups onto the OCMK-3 surface, which were favorable for catalytic activation of PS (Liu and Xiong et al., 2019).

3.2. Catalytic performances of OCMK-3

It has been reported that high concentration of acid treatment might lead to collapse of the pore structure of the carbonaceous material, and excessive oxygen-containing functional groups could block the micropores and thus reduce the specific surface area and pore capacity, which might inhibit the oxidative degradation activity of the catalysts(Bazu A and Lu et al., 2008). To obtain the optimum conditions for OMCK-3 synthesis for CIP removal, CIP removal experiments were performed using OCMK-3 prepared under various conditions, with the results shown in Tables S1-S3. Compared with the pristine CMK-3, both the adsorption and removal of ciprofloxacin of OCMK-3 could be enhanced only after treatment with 4 mol/L of nitric acid solution. As shown in Table S2, neither the adsorption capacity nor the catalytic efficiency of OCMK-3 could get enhanced when the synthetic temperature was 70℃ or 90℃. And Table S3 indicated that both of the adsorption and catalytic performance experienced a rise when the modification time increased from 15 min to 45 min, but started to decrease when the time increased to 60min. Therefore, compared with the pristine CMK-3, the adsorption and catalytic performance of OCMK-3 could be enhanced under certain synthetic conditions.

In practical application, the catalytic performance of the OCMK-3/PS system is often affected by environmental parameters. Therefore, the removal efficiency of CIP and the corresponding kinetic performance were studied by changing reaction parameters (e. g. the dosage of OCMK-3 and persulfate, solution pH and CIP initial concentration, temperature and coexistent ions). Firstly, the effect of the dosage of OCMK-3 was investigated, with the results shown in Fig. 5(a). PS alone could hardly oxidize CIP without activation, with the removal rate only about 8%. Herein, with the increase of dosage from 0.1g/L to 0.4g/L, the removal efficiency of CIP was enhanced, which could be attributed to more activators and active sites provided by the increased amounts of OCMK-3. However, k_{obs} did not increase when the dose of OCMK-3 was above 0.3g/L, which might be limited by the dose of PS. The influence of the PS dosage was also investigated. First, in order to eliminate the influence of adsorption, the adsorption experiment was carried out for 3h without the addition of PS. As shown in Fig. 5(b), the adsorption process reached equilibrium within 1h and about 40% of CIP was removed. After adsorption reached equilibrium at 1h, PS was added. It could be observed from Fig. 5(b) that the concentration of CIP decreased significantly. It means that in addition to adsorption, chemical reactions were also involved in the system, which was affected by the PS dosage. The Langmuir-Hinshelwood (L-H) kinetic model was used to fit the removal curve of CIP. Formula (1) and (2) are (L-H) variable forms.

$$-\frac{dC}{dt} = K_{obs}C$$

1

$$In\left(\frac{C_t}{C_o}\right) = -K_{obs}t$$

2

where C_0 and C_t are the concentrations of CIP, Kobs is the pseudo-first-order reaction rate constant (min^{-1}), and it is the reaction time (min).

When the PS dosage rose from 2mM to 8mM, K_{obs} increased from 0.00189 / min to 0.00364 / min. An increase in K_{obs} at the beginning might be resulted from more reactive free radicals through increasing PS dosage. However, K_{obs} decreased when PS dosage continued to increase, which could be due to the self-quenching effect between excessive free radicals(Guo and Zeng et al., 2017).

The effect of pH on the removal of CIP was studied over the pH range of 3.0 and 5.0, as such concentration of CIP was insoluble under neutral and alkaline conditions. As shown in Fig. 5 (d), the maximum removal of CIP occurred when pH was 4. To further understand the effects of pH, zeta potential for OCMK-3 under various pH values was analyzed. As shown in Fig. 5 (c), the isoelectric point of OCMK-3 is 2.1. Thus when the solution pH is more than 2.1, the surface of OCMK-3 is negatively charged(Saleh and Isik et al., 2021). When the solution pH was 3 or 4, CIP existed as cationic form CIP^+ as a result of the protonation of the secondary amine on the piperazine group, while OCMK-3 surface was oppositely charged. However, OCMK-3 was more negatively charged when pH was 4, resulting in the enhanced adsorption amounts. When pH reached 5, CIP could exist as zwitterionic ($CIP^{\pm}$). In this stage, both CIP molecules and OCMK-3 surfaces were negatively charged, resulting in depressed adsorption process(Peng and Hu et al., 2015).

As demonstrated in Fig. 6 (a), CIP removal efficiency decreased from 89–57% with the increase of CIP concentration from 100mg/L to 300mg/L. As the concentration of pollutants rose, the increased competition of CIP molecules might be the reason for the reduced removal rate(Ye and Yan et al., 2019; Ahammad and Zulkifli et al., 2021).

To compare CIP removal by the prepared CMK-3 and OCMK-3, comparative experiments were carried out, with the results described in Fig. 6 (b). About 42% and 74% of CIP were removed in 3 h by CMK-3 and OCMK-3, respectively. The removal efficiency of OCMK-3 was about 1.76 times that of CMK-3, which further verified that oxidation treatment could increase the activity of the catalyst. To evaluate the oxidative degradation performance, the mineralization degree of organic contaminants was investigated. It could be clearly observed from Fig. 6 (c) that TOC removal by the OCMK-3/PS system was about 11% higher than that by the CMK-3/PS system. This suggested that the OCMK-3/PS system could not only enhance the removal of CIP but also exhibited higher mineralization efficiency.

The effects of temperature on CIP removal were further investigated, with the results shown in Fig.S2(a). At 25℃, 74% of CIP could be removed. When the temperature increased to 45℃, about 81% of CIP could be removed. Thus it could be inferred that elevated temperatures could lead to enhanced PS activation. There might be two reasons to interprete this phenomenon. Firstly, higher temperature could facilitate the decomposition of PS and therefore accelerated the removal of CIP. Secondly, the elevated temperature could also promote the adsorption process, which was favorable for the electron transfer between OCMK-3 and PS (Tang and Liu et al., 2018).

The trace amounts of inorganic anions often existed in real wastewaters, which might affect catalytic behaviors in very complex ways. Fig.S2(b, c) showed the effects of the different concentrations of HCO_3^- and Cl^- on CIP removal. As shown in Fig.S2(b), when the HCO_3^- concentration rose from 0 to 10 mM, the removal of CIP was also increased. The reason for the increase might lie in that the addition of HCO_3^- might increase the solution pH, thus reduced the solubility of CIP molecules(Wu and Li et al., 2013). However, when the HCO_3^- concentration rose to 20 mM, CIP removal efficiency slightly decreased. As HCO_3^- could act as an electron donor, it might compete with CIP for reacting with $SO_4\cdot^-$ thus hindered CIP removal (Eqs. (3)-(4))(Wen and Qiang et al., 2018; Yong and Jie et al., 2018).

$$SO_4 \bullet^- + HCO_3^- \rightarrow HCO_3 \bullet^- + SO_4^{2-}$$

3

$$\bullet OH + HCO_3^- \rightarrow OH^- + HCO_3 \bullet^-$$

4

As demonstrated in Fig.S2 (c.), the presence of 5mM and 10mM chlorides slightly decreased the remove rate, as Cl^- could act as radical scavengers and combine with $SO_4\cdot^-$ and ·OH to generate Cl· and $Cl_2\cdot^-$ (Eqs. (5)-(8))(Guo and Yan et al., 2021). Whereas, an obvious increase of kobs could be observed with the chloride concentration continued to increase to 20 mM. Herein, besides scavenging $SO_4\cdot^-$ and ·OH, super abundant Cl^- could also take part in the removal of CIP, which might act as an electron donor to afford electrons to PS, thus the active chlorine species and sulfate radicals were generated under the catalysis of OCMK-3(Anipsitakis and Dionysiou et al., 2006; Oyekunle and Cai et al., 2021).

$$SO_4 \bullet^- + Cl^- \rightarrow Cl \bullet + SO_4^{2-}$$

5

$$\bullet OH + Cl^- \rightarrow ClOH \bullet^-$$

6

$$ClOH \bullet^- + H^+ \rightarrow Cl \bullet + H_2O$$

7

$$Cl \bullet + Cl^- \rightarrow Cl_2 \bullet^-$$

8

3.3. Identification of radicals

Herein, to investigate the effects of radicals, radical quenching reaction was analyzed. $SO_4\cdot^-$and ·OH have been regarded as two typical reactive species involved in PS activation. Studies had demonstrated the strong quenching ability of Methanol for ·OH ($k_{\cdot OH}=9.7\times10^8 M^{-1}s^{-1}$, $kSO_4\cdot^- =3.2\times10^6 M^{-1}s^{-1}$), while EtOH served as an effective quencher for $SO_4\cdot^-$ ($k_{\cdot OH} = (1.6\text{-}7.8)\times10^7 M^{-1}s^{-1}$, $kSO_4\cdot^- = (1.2\text{-}2.8)\times10^9 M^{-1}s^{-1}$) (Buxton and Greenstock et al., 1988). Thus Methanol and EtOH were utilized as quenchers, with the results shown in Fig. 7 (a-b). The CIP removal was restrained from the existence of either MeOH or EtOH, with a decrease of kobs from 0.0044 min^{-1} to 0.00131 min^{-1}(n[MeOH/PS] = 1000) and 0.00134 min^{-1}(n[EtOH/PS] = 1000), respectively. It could be referred that both $SO_4\cdot^-$and ·OH were generated and involved in the reaction. In addition, 1,4-benzoquinone (BQ) was introduced as a quencher to identify the existence of superoxide anion radicals ($O_2\cdot^-$), with the results shown in Fig. 7 (c). Slight inhibition in the reaction by BQ could be observed, with a decrease of kobs from 0.0044 min^{-1} to 0.0034 min^{-1}, indicating that $O_2\cdot^-$ was also involved in CIP removal.

Electron paramagnetic resonance (EPR) spectroscopy was employed to further con□rm the existence of radicals. Fig. 7 (d) shows the characteristic peaks of DMPO·OH (hyperfine splitting constants of aN = aH = 14.9 G) and DMPO·SO_4(aN = 13.2 G, aH = 9.6 G, aH = 1.48 G and aH = 0.78 G) (Wang and Sun et al., 2015), in agreement with the quenching experiment, and it could be further inferred that ·OH and SO4·$^-$ were involved in the reaction(Jiang and Li et al., 2020). Meanwhile, six characteristic peaks of DMPO-$O_2\bullet^-$ could be observed in Fig. 7. (e), further confirming the occurrence of $O_2\cdot^-$(Wang and Lin et al., 2017; Cdab and Zhuo et al., 2021).

3.4. Degradation products and pathways

In this study, 9 transformation intermediates of CIP were identified by the LC-MS technique (Table S2 and Fig.S3). Through interpreting the molecular ion masses, analyzing ESI(+) MS spectra and comparing with previous studies (Guo and Li, 2013; Guo and Gao et al., 2016), three major reaction pathways for CIP degradation were proposed and were illustrated in Fig. 8.

Pathway I was initiated by cleaving piperazine ring, and then ·OH, SO4·$^-$, and $O_2\cdot^-$ attack caused stepwise oxidation This route in agreement with the study that the piperazine ring was determined to be the most active site for the free radical attack(Jiang and Ji et al., 2016). Oxidation of piperazine led to ring opening, resulting in the dialdehyde derivative C1. C1 converted into C2 through removing one formaldehyde from the open piperazine ring, and then transformed into C3 through further loss of second formaldehyde in the open piperazine ring. The compound C3 could be further oxidized into C4 by losses of secondary amine nitrogen(Mahdi-Ahmed and Chiron, 2014).

In Pathway □, CIP was firstly converted to C5 by hydroxylation, and then transformed into C6 through OH/F substitution and further hydroxylation. C7 was formed by substituting -COOH with -OH in C6. This pathway was also proposed in other studies(Zhu and Wang et al., 2019).

In Pathway Ⅲ, CIP might convert into C8 by defluorination. On the one side, product C9 was produced through piperazine epoxidation from C8. On the other side, the C8 might also form C5, through hydroxylation, and then with the similar route to pathway II, through further hydroxylation and decarboxylation process were similar to pathway II, the same intermediate C6 and C7 was generated. This pathway in agreement with that proposed by Yja, B., et al.(Yja and Cf et al., 2014).

3.5. Electron transfer pathways

Based on the above analysis, the mechanism of CIP removal using the OCMK-3/PS system was proposed and shown in Scheme 1. The unique electronic circumstance on the surface of OCMK-3, resulted in the defective edge sites and free-flowing π electrons of the sp2-hybridized carbon network, which might impose effects on the electron configuration of PS and weaken the O-O bond to generate metastable complexes(Duan and Sun et al., 2015). In addition, the large specific surface area and porous structure of OCMK-3 could facilitate the adsorption of PS and CIP molecules onto its surface, and thus promoted their contact and subsequent reactions. Accordingly, two possible pathways were proposed in the following evolution.

The radical pathway: PS was easily hydrolyzed by the metastable complex (Eq. (9)), and then the oxidation between HO_2^- and $S_2O_8^{2-}$ occurred via one-electron transfer process, leading to the generation of $SO_4\cdot^-$ and $O_2\cdot^-$(Eq. (10)). $SO_4\cdot^-$ could also convert to ·OH via Eq. (11). Here, OCMK-3 played a vital role as the electron transfer mediator(Jya and Xh et al., 2020). The generated $SO_4\cdot^-$, ·OH and $O_2\cdot^-$ could then participated in the degradation of CIP(Duan and Sun et al., 2018).

The nonradical pathway: In PS nonradical activation systems, when the electron-rich CIP molecule approached the activated PS molecule, a ternary system of electron donor (CIP)-mediator (OCMK-3)-acceptor (PS) was established. PS was used up in CIP oxidation by getting two electrons from organics (Eq. (12)(Yao and Zhang et al., 2019)), and the radical reactions did not occur due to the steady state of PS (Chen and Ma et al., 2019; Zhang and Tang et al., 2020).

The radical and nonradical oxidation processes both took part in the reaction in this system. OCMK-3 acted as an electron transfer mediator, which could facilitate the transfer of electrons from CIP or H_2O to PS. The electron transfer pathways were conformed to the CMK-3/PS system studied previously(Tang and Liu et al., 2018; Liu and Lai et al., 2019), indicating that OCMK-3 did not change the degradation pathway.

$$S_2O_8^{2-} + 2H_2O \rightarrow HO_2^- + 2SO_4^{2-} + 3H^+$$

9

$$S_2O_8^{2-} + HO_2^- \rightarrow SO_4\bullet^- + SO_4^{2-} + O_2\bullet^- + H^+$$

10

$$SO_4 \bullet^- + OH^- \rightarrow SO_4^{2-} + \bullet OH$$

11

$$S_2O_8^{2-} + 2e^- \rightarrow 2SO_4^{2-}$$

12

3.6. Stability of OCMK-3 and Real wastewater application

The stability of the catalyst OCMK-3 for continuous PS activation was evaluated for further application. The experiment was carried out for four cycles to test the reusability of OCMK-3, with the results shown in Fig.S4. A slight decrease in CIP removal efficiency could be observed after each cycle, which might be attributed to the oxidation of the surface during the reaction, which changed its chemical composition. Moreover, the interaction between PS and the active sites was hindered owing to the adsorption of oxidation intermediates, thus imposing effects on the surface chemistry of OCMK-3 and the electron transfer from OCMK-3 to PS. However, the CIP removal by regenerated OCMK-3 after four cycles was 89.2% of that by the fresh OCMK-3, demonstrating that OCMK-3 could be regenerated and reused(Jya and Xh et al., 2020).

To test the practicability of the OCMK-3/PS system, real pharmaceutical wastewater was used as a target to test the degradation efficiency of the OCMK-3/PS system in the complex environment, with the results shown in Fig. 9. Multiple peaks could be observed from the spectrum of the original sample in Fig. 9 (a), showing complex components of the water with high concentrations. The high fluorescence intensities could also be identified in Fig. 9 (a), which were related to fulvic-like compounds, indicating the poor biodegradability and serious pollution of the wastewater(Wang and Yang et al., 2016). After the adsorption, the number and area of peaks in Fig. 9 (b) were reduced, indicating that most fulvic-like compounds were adsorbed by OCMK-3. After two hours of reaction with OCMK-3/PS (Fig. 9 (c)), peaks were almost disappeared, indicating that the dissolved organic matter was almost removed after treatment, and the biodegradability of water was greatly improved(Yu and Feng et al., 2020). In addition, to further evaluate the mineralization of the organics, TOC contents of the wastewater were evaluated, with the results shown in Fig. 9 (d). It could be observed that only 5% of TOC were adsorbed, while about 75% of TOC were removed in OCMK-3/PS system, indicating the high TOC removal efficiency of the system. The results further convinced the high removal efficiency of the OCMK-3/PS system in both laboratory-prepared polluted water and practical wastewater.

4. Conclusions

In this study, a novel carbon catalyst, OMCK-3 was synthesized for the activation of persulfate to remove CIP. Compared with CMK-3, OCMK-3 exhibited higher CIP removal efficiency. The introduction of oxygen-containing groups increased the specific surface area and pore volume, provided multiple oxygen-containing groups and good electron transfer ability, thus resulted in the excellent adsorption performance and catalytic performance of OMCK-3. During CIP degradation, various intermediates were

identified and the degradation pathways were proposed. Both radical and nonradical pathways were involved in the oxidation process of CIP, and OCMK-3 acted as a mediator to promote the electron transfer between CIP (electron donor) and PS (electron acceptor), leading to the oxidative degradation of CIP. Additionally, the actual treatment of pharmaceutical wastewater using the OCMK-3/PS system further proved its high efficiency in organic wastewater treatment.

Declarations

Acknowledgement

The study was financially supported by National Key R&D Program of China (2017YFC0505606), the National Natural Science Foundation of China (51609023), Natural Science Foundation of Hunan Province (2017JJ3328), National Social Science Foundation of China (15BJY051), Water Conservancy Science and Technology Project of Hunan Province (2015-245-19), Scientific Research Project of Education Department of Hunan province (19C0039), and the authors would like to appreciate the help of XPS test from Shiyanjia Lab(www.shiyanjia.com).

Authors contributions

Ying Xiong：Resources, Supervision, Funding acquisition, Writing - Review and Editing.

Xiaolei Dai: Formal analysis, Visualization, Investigation, Writing- Original draft preparation.

Yuanyuan Liu: Conceptualization, Project administration, Methodology, Analysis and Writing- Reviewing and Editing.

Chunyan Du：Validation, Writing- Reviewing and Editing.

Guanlong Yu: Validation, Writing- Reviewing and Editing.

Yan Xia：Investigation.

Availability of data and materials

All data generated or analyzed during this study are included in this published article.

Ethics approval and consent to participate Not applicable.

Consent for publication Not applicable.

Competing interests The authors declare no competing interests.

References

1. Ahammad NA, Zulkifli MA et al (2021) Desorption of chloramphenicol from ordered mesoporous carbon-alginate beads: Effects of operating parameters, and isotherm, kinetics, and regeneration studies. Journal of Environmental Chemical Engineering 9(1):105015
2. Anipsitakis GP, Dionysiou DD et al (2006) "Cobalt-mediated activation of peroxymonosulfate and sulfate radical attack on phenolic compounds. implications of chloride ions" Environmental Science Technology 40(3):1000–1007
3. Anjali R, Shanthakumar S (2019) Insights on the current status of occurrence and removal of antibiotics in wastewater by advanced oxidation processes. J Environ Manage 246:51–62
4. Bazu A, P. A. and Lu AH et al (2008) Surface and pore structure modification of ordered mesoporous carbons via a chemical oxidation approach. Microporous Mesoporous Materials 108(1-3):266–275
5. Buxton GV, Greenstock CL et al (1988) Critical Review of Rate Constants for Reactions of Hydrated Electrons, Hydrogen Atoms and Hydroxyl Radicals (OH/O) in Aqueous Solution. J Phys Chem Ref Data 17(2):513–886
6. Cdab C, Zhuo ZA et al (2021) "Construction of Z-scheme g-C 3 N 4 / MnO 2 /GO ternary photocatalyst with enhanced photodegradation ability of tetracycline hydrochloride under visible light radiation." Environmental Research
7. Chen C, Ma T et al (2019) In-situ pyrolysis of Enteromorpha as carbocatalyst for catalytic removal of organic contaminants: Considering the intrinsic N/Fe in Enteromorpha and non-radical reaction. Appl Catal B 250:382–395
8. Cuerda-Correa, Alexandre-Franco et al (2019) "Advanced Oxidation Processes for the Removal of Antibiotics from Water. An Overview" Water 12(1):102
9. Du C, Zhang Z et al (2021) A review of metal organic framework (MOFs)-based materials for antibiotics removal via adsorption and photocatalysis. Chemosphere 272(12):129501
10. Du J, Zhang Y et al (2020) "N/B-co-doped ordered mesoporous carbon spheres by ionothermal strategy for enhancing supercapacitor performance. " Journal of Colloid and Interface Science
11. Duan, Xiaoguang et al (2018) Metal-free activation of persulfate by cubic mesoporous carbons for catalytic oxidation via radical and nonradical processes. Catal Today 307:140–146
12. Duan X, Su C et al (2016) Surface controlled generation of reactive radicals from persulfate by carbocatalysis on nanodiamonds. Applied Catalysis B Environmental 194:7–15
13. Duan X, Sun H et al (2015) "Insights into Heterogeneous Catalysis of Persulfate Activation on Dimensional-Structured Nanocarbons. " Acs Catalysis 5(8):4629–4636
14. Duan X, Sun H et al (2018) "Nonradical reactions in environmental remediation processes: Uncertainty and challenges". Appl Catal B 224:973–982
15. Fonseca RF, De G (2020) "Modeling Anaerobic Digestion Metabolic Pathways for Antibiotic-Contaminated Wastewater Treatment. " Biodegradation 31:4–6

16. Furman OS, Teel AL et al (2010) "Mechanism of Base Activation of Persulfate" Environmental Science Technology 44(16):6423–6428
17. Gómez-Serrano V, Piriz-Almeida F et al (1999) Formation of oxygen structures by air activation. A study by FT-IR spectroscopy. Carbon 37(10):1517–1528
18. Guo H, Gao N et al (2016) "Kinetics and Transformation Pathways on Oxidation of Fluoroquinolones with Thermally Activated Persulfate". Chem Eng J 292:82–91
19. Guo ONGW, Li L (2013) Photochemical degradation of ciprofloxacin in UV and UV/H 2 O 2 process: kinetics, parameters, and products. Environ Sci Pollut Res 20(5):3202–3213
20. Guo Y, Yan L et al (2021) Goethite/biochar-activated peroxymonosulfate enhances tetracycline degradation: Inherent roles of radical and non-radical processes. Science of The Total Environment 783(100076):147102
21. Guo Y, Zeng Z et al (2017) "Catalytic oxidation of aqueous organic contaminants by persulfate activated with sulfur-doped hierarchically porous carbon derived from thiophene." Applied Catalysis B: Environmental: 635–644
22. Guo Y, Zeng Z et al (2017) Catalytic oxidation of aqueous organic contaminants by persulfate activated with sulfur-doped hierarchically porous carbon derived from thiophene. Appl Catal B 220:635–644
23. Hao C, Carroll KC (2016) Metal-free catalysis of persulfate activation and organic-pollutant degradation by nitrogen-doped graphene and aminated graphene. Environ Pollut 215:96–102
24. Indrawirawan S, Sun H et al (2015) Nanocarbons in different structural dimensions (0–3D) for phenol adsorption and metal-free catalytic oxidation. Applied Catalysis B Environmental 179:352–362
25. Jiang C, Ji Y et al (2016) Sulfate radical-based oxidation of fluoroquinolone antibiotics: Kinetics, mechanisms and effects of natural water matrices. Water Res 106(dec.1):507–517
26. Jiang Z, Li J et al (2020) Removal of atrazine by biochar-supported zero-valent iron catalyzed persulfate oxidation: Reactivity, radical production and transformation pathway. Environ Res 184:109260
27. Jun S (2000) Synthesis of new, nanoporous carbon with hexagonally ordered mesostructure. J Am Chem Soc 122:10712–10713
28. Jya B, Xh A et al (2020) "Electron-transfer-dominated non-radical activation of peroxydisulfate for efficient removal of chlorophenol contaminants by one-pot synthesized nitrogen and sulfur codoped mesoporous carbon." Environmental Research 194
29. Jya B, Xh A et al (2020) Electron-transfer-dominated non-radical activation of peroxydisulfate for efficient removal of chlorophenol contaminants by one-pot synthesized nitrogen and sulfur codoped mesoporous carbon. Environ Res 194:110496
30. Kim W, Kang MY et al (2011) Preparation of nanoporous carbons via a grafting method for the application to electrochemical double layer capacitors. J Nanosci Nanotechnol 11(1):751–754

31. Li H, Di Z et al (2014) Adsorption of antibiotic ciprofloxacin on carbon nanotubes: pH dependence and thermodynamics. Chemosphere 95(jan.):150–155
32. Li X, Zhou M et al (2017) Highly efficient advanced oxidation processes (AOPs) based on pre-magnetization Fe0 for wastewater treatment. Sep Purif Technol 178:49–55
33. Liu N, Jin X et al (2015) Pharmaceuticals and Personal Care Products(PPCPs) Caused Reproductive Toxicity in Surface Water of China: A Review. Asian Journal of Ecotoxicology 10(06):1–12
34. Liu S, Lai C et al (2019) "Role of radical and non-radical pathway in activating persulfate for degradation of p-nitrophenol by sulfur-doped ordered mesoporous carbon". Chem Eng J 384:123304
35. Liu Y, Xiong Y et al (2019) Enhancement of Pb (II) adsorption by Boron doped ordered mesoporous carbon: Isotherm and kinetics modeling. Science of The Total Environment 708:134918
36. Mahdi-Ahmed M, Chiron S (2014) Ciprofloxacin oxidation by UV-C activated peroxymonosulfate in wastewater. J Hazard Mater 265:41–46
37. Matzek LW, Carter KE (2016) Activated persulfate for organic chemical degradation: A review. Chemosphere 151(May):178–188
38. Meena VD, Dotaniya ML et al (2015) Antibiotics and antibiotic resistant bacteria in wastewater: Impact on environment, soil microbial activity and human health. African Journal of Microbiology Research 9(14):965–978
39. Mueller E, Schuessler W et al (2013) Aerobic biodegradation of the sulfonamide antibiotic sulfamethoxazole by activated sludge applied as co-substrate and sole carbon and nitrogen source. Chemosphere 92(8):969–978
40. Mushtaque and Ahmad, et al (2013) "Mechanism of Persulfate Activation by Phenols. " Environmental Science Technology: ES&T 47(11):5864–5871
41. Nejad NF, Shams E et al (2016) "Efficient desulfurization of fuel with functionalized mesoporous carbon CMK-3-O and comparison its performance with mesoporous carbon CMK-3". Fullerene Science Technology 24(12):786–795
42. Oyekunle DT, Cai J et al (2021) "Impact of Chloride ions on activated Persulfates based Advanced Oxidation Process (AOPs): A Mini. Review" Chemosphere 280:130949
43. Peng X, Hu F et al (2015) "Adsorption behavior and mechanisms of ciprofloxacin from aqueous solution by ordered mesoporous carbon and bamboo-based carbon. " Journal of Colloid and Interface Science
44. Saleh M, Isik Z et al (2021) "Green synthesis of zero valent iron nanoparticles using Verbascum Thapsus and its Cr (VI) reduction activity". Bioresource Technology Reports 13:100637
45. Shao P, Duan X et al (2017) Heterogeneous activation of peroxymonosulfate by amorphous boron for degradation of bisphenol S. J Hazard Mater 322:532–539
46. Su HC, Pan CG et al (2014) Contamination profiles of antibiotic resistance genes in the sediments at a catchment scale. Science of The Total Environment 490C:708–714

47. Tang L, Liu Y et al (2018) "Enhanced activation process of persulfate by mesoporous carbon for degradation of aqueous organic pollutants: Electron transfer mechanism." Applied Catalysis B: Environmental: 1–10
48. Tello A, Austin B et al (2012) "Selective Pressure of Antibiotic Pollution on Bacteria of Importance to Public Health". Environ Health Perspect 120(8):1100–1106
49. Thanekar P, Panda M et al (2018) Degradation of carbamazepine using hydrodynamic cavitation combined with advanced oxidation processes. Ultrason Sonochem 40(Pt A):567–576
50. Torres-Perez J, Gerente C et al (2012) Sustainable Activated Carbons from Agricultural Residues Dedicated to Antibiotic Removal by Adsorption. Chin J Chem Eng 20(003):524–529
51. Tran TV, Nguyen D et al (2019) MIL-53 (Fe)-directed synthesis of hierarchically mesoporous carbon and its utilization for ciprofloxacin antibiotic remediation. Journal of Environmental Chemical Engineering 7(1):102881
52. Vara H, Collazos-Castro JE (2019) "Enhanced spinal cord microstimulation using conducting polymer-coated carbon microfibers. " Acta Biomaterialia
53. Wang J, Zhuan R (2019) Degradation of antibiotics by advanced oxidation processes: An overview. Science of The Total Environment 701:135023
54. Wang J, Lin T et al (2017) "0D/2D interface engineering of carbon quantum dots modified Bi2WO6 ultrathin nanosheets with enhanced photoactivity for full spectrum light utilization and mechanism insight." Applied Catalysis B Environmental 222
55. Wang L, Yang Q et al (2016) Advanced landfill leachate treatment using iron-carbon microelectrolysis- Fenton process: Process optimization and column experiments. J Hazard Mater 318(NOV.15):460–467
56. Wang Y, Sun H et al (2015) "3D-hierarchically structured MnO2 for catalytic oxidation of phenol solutions by activation of peroxymonosulfate: Structure dependence and mechanism". Applied Catalysis B Environmental 164:159–167
57. Wang Y, Man L et al (2018) Insights into heterogeneous catalysis of peroxymonosulfate activation by boron-doped ordered mesoporous carbon. Carbon 135:238–247
58. Wen G, Qiang C et al (2018) "Bromate formation during the oxidation of bromide-containing water by ozone/peroxymonosulfate process: Influencing factors and mechanisms". Chem Eng J 352(15):316–324
59. Wu Q, Li Z et al (2013) Desorption of ciprofloxacin from clay mineral surfaces. Water Res 47(1):259–268
60. Xu C, Farber M et al (2003) Mechanisms of surfactant adsorption on non-polar, air-oxidized and ozone-treated carbon surfaces. Carbon 41(8):1489–1500
61. Yang S, Li L et al (2016) "Role of surface chemistry in modified ACF (activated carbon fiber)-catalyzed peroxymonosulfate oxidation". Appl Surf Sci 383(oct.15):142–150

62. Yang S, Chen Y et al (2008) A novel advanced oxidation technology based on activated persulfate. Progress in Chemistry 20(9):1433–1438
63. Yao C, Zhang Y et al (2019) "Insights into the mechanism of non-radical activation of persulfate via activated carbon for the degradation of p -chloroaniline". Chem Eng J 362:262–268
64. Ye S, Yan M et al (2019) "Facile assembled biochar-based nanocomposite with improved graphitization for efficient photocatalytic activity driven by visible light. " Applied Catalysis B: Environmental
65. Yja B, Cf B et al (2014) Degradation of ciprofloxacin and sulfamethoxazole by ferrous-activated persulfate: Implications for remediation of groundwater contaminated by antibiotics. Science of The Total Environment 472:800–808
66. Yong L, Jie L et al (2018) "Enhanced degradation of isoproturon in soil through persulfate activation by Fe-based layered double hydroxide: different reactive species comparing with activation by homogenous Fe(II). " Environmental Science & Pollution Research, pp 1–11
67. Yu J, Feng H et al (2020) Insight into the key factors in fast adsorption of organic pollutants by hierarchical porous biochar. J Hazard Mater 403:123610
68. Zhang H, Tang L et al (2020) Enhanced surface activation process of persulfate by modified bagasse biochar for degradation of phenol in water and soil: Active sites and electron transfer mechanism. Colloids Surfaces A Physicochemical Engineering Aspects 599:124904
69. Zhu D, Wang Y et al (2015) Nitrogen-containing carbon microspheres for supercapacitor electrodes. Electrochim Acta 158(Complete):166–174
70. Zhu S, Wang W et al (2019) "Iron sludge-derived magnetic Fe0/Fe3C catalyst for oxidation of ciprofloxacin via peroxymonosulfate activation". Chem Eng J 365:99–110
71. Zolfaghari G, Esmaili-Sari A et al (2011) Surface Modification of Ordered Nanoporous Carbons CMK-3 via a Chemical Oxidation Approach and its Application in Removal of Lead Pollution from Water. Proceedings of International Conference on Environmental Science and Technology(ICEST 2011)

Scheme

Schemes 1 is available in the Supplementary Files section.

Figures

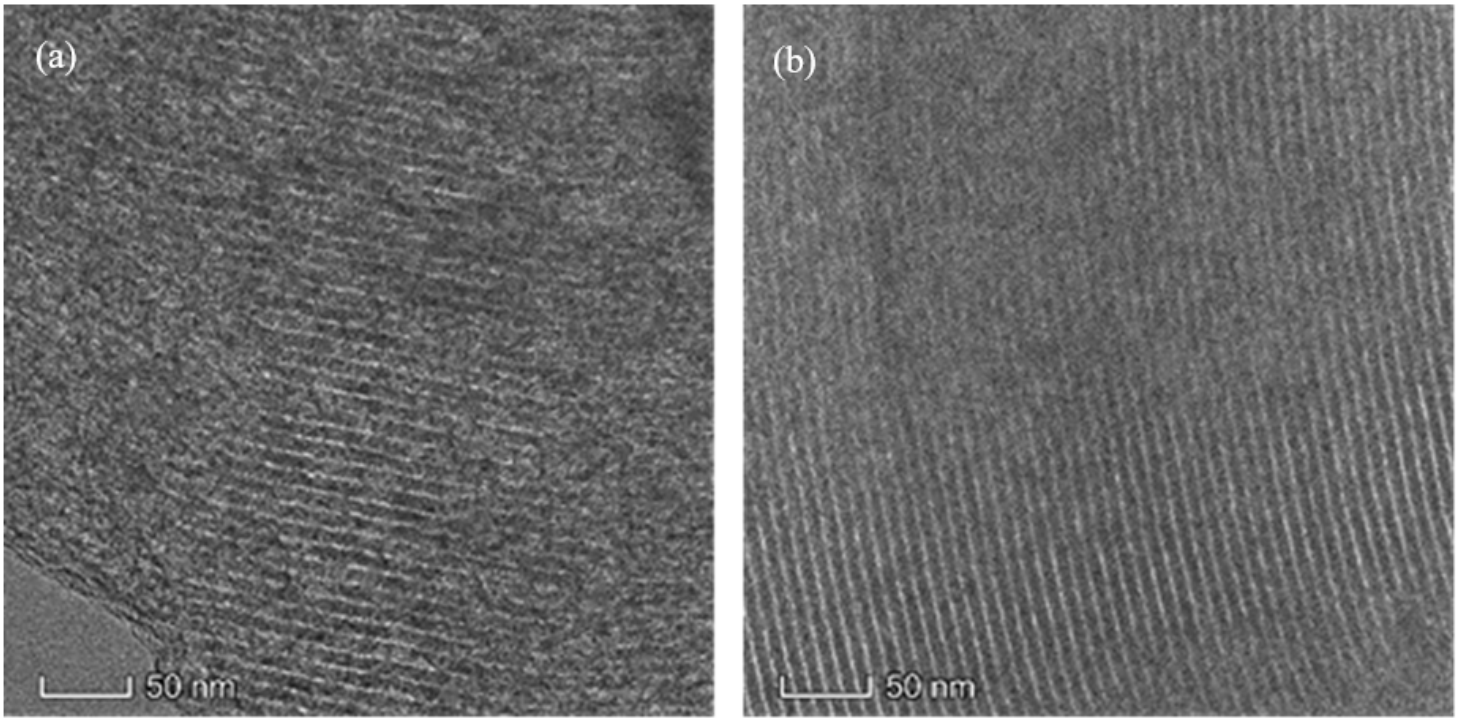

Figure 1

TEM images of (a) OMC and (b) OCMK-3.

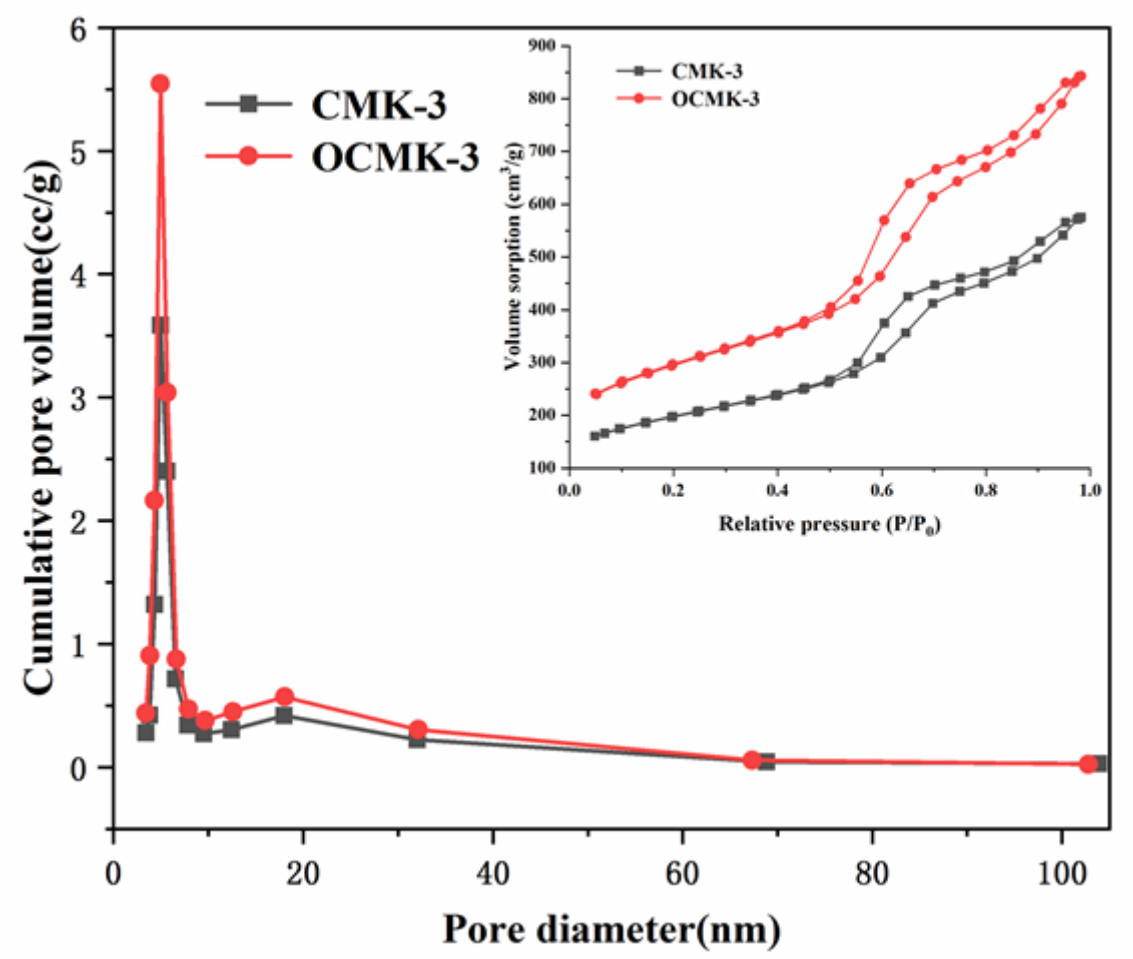

Figure 2

Nitrogen adsorption-desorption isotherms and the corresponding pore size distributions of CMK-3 and OCMK-3 (inset).

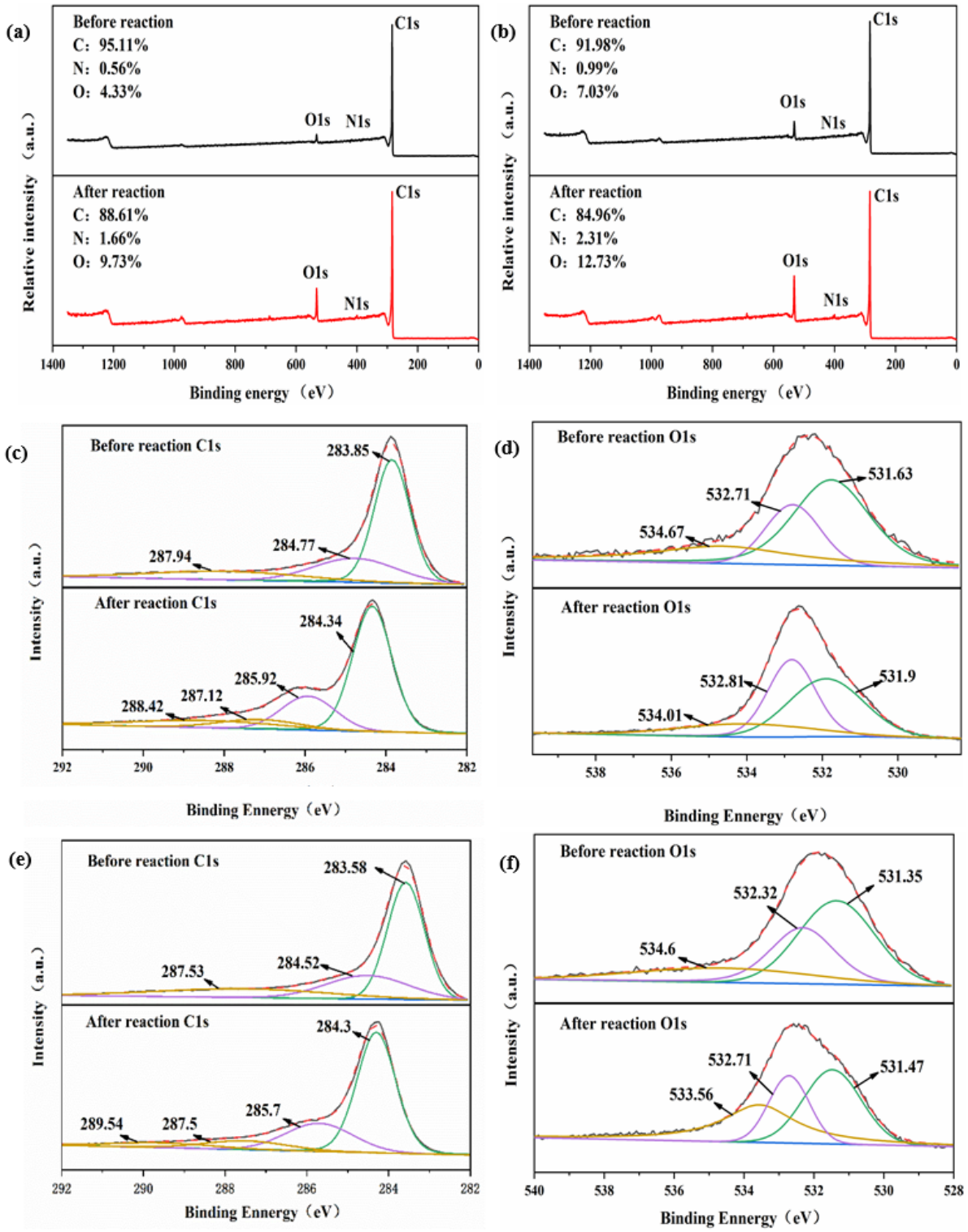

Figure 3

(a)XPS survey of CMK-3 before and after reaction; (b) XPS survey of OCMK-3 before and after reaction;(c) C1s and (d) O1s high resolution scans of CMK-3 before and after reaction;(e) C1s and (f) O1s high resolution scans of OCMK-3 before and after reaction.

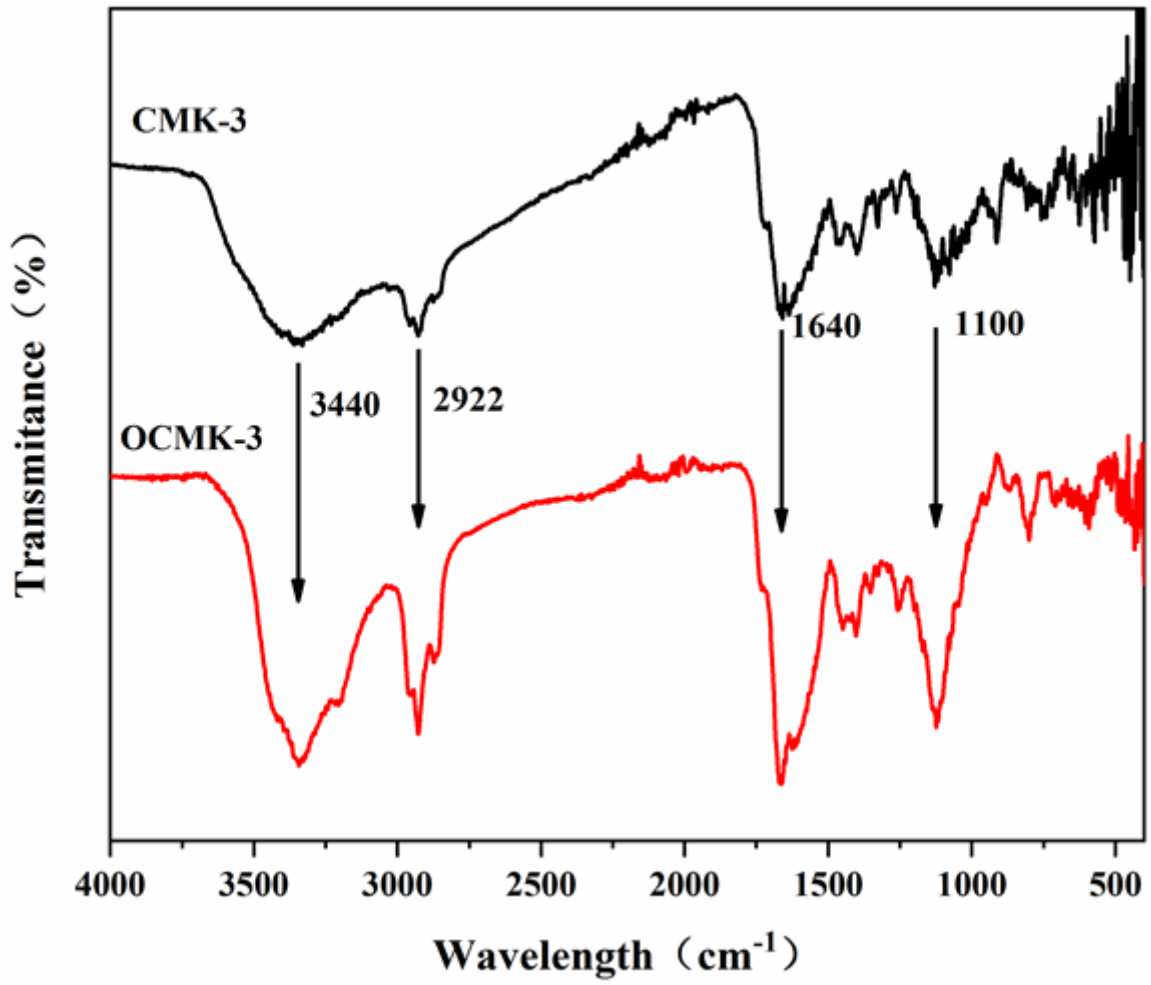

Figure 4

Fourier transform-infrared (FTIR) spectra of CMK-3 and OCMK-3.

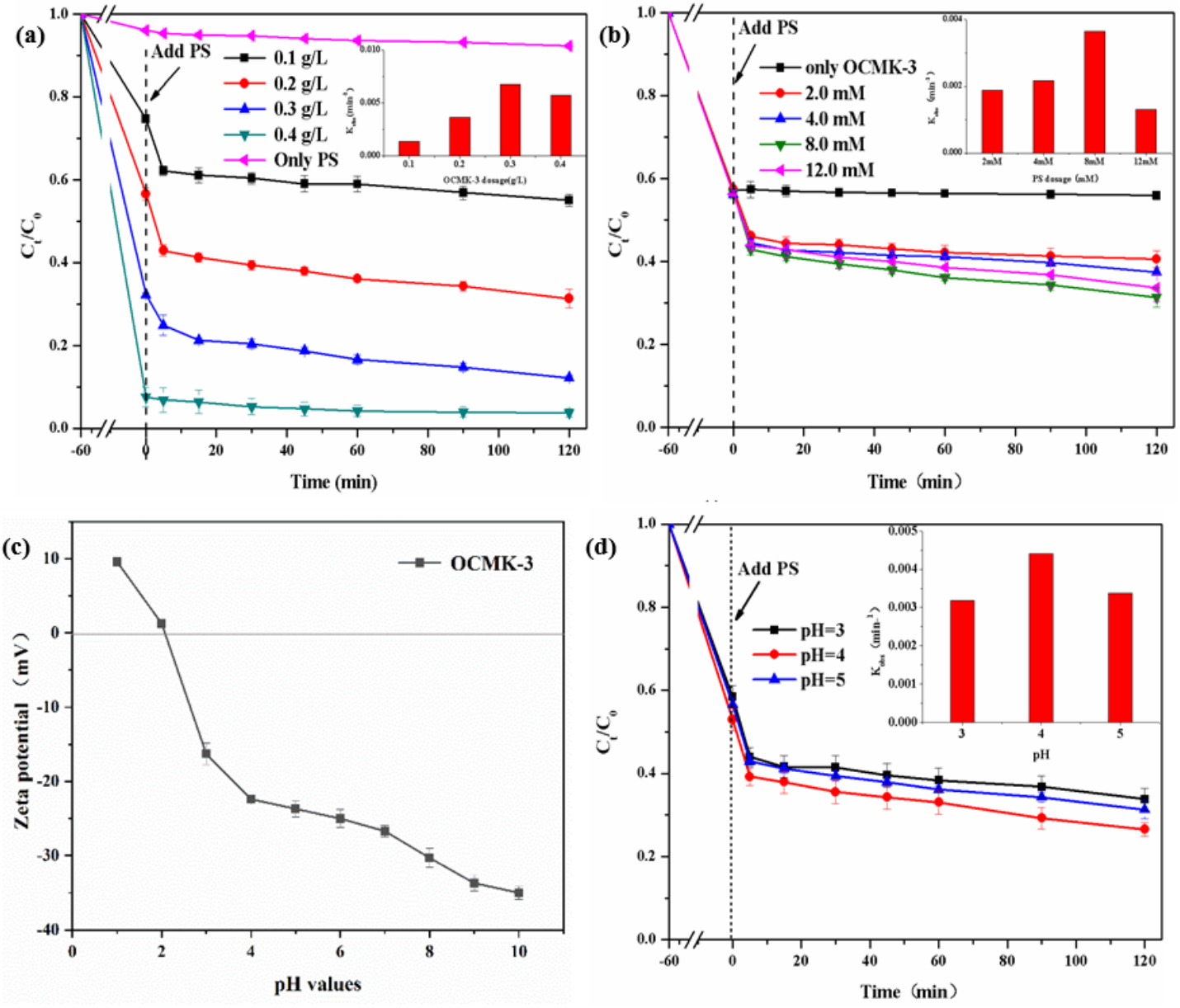

Figure 5

The effects of (a) OCMK-3 dosage ([PS] = 8 mM) and (b) PS dosage ([CMK-3] = 0.2 g/L) on CIP removal. (c) Zeta potential of OCMK-3; (d) effect of pH on CIP removal by OCMK-3. (Insets are the corresponding changes of pseudo-first-order rate constant). Conditions: [CIP]=200mg/L, [Temp]=25°C.

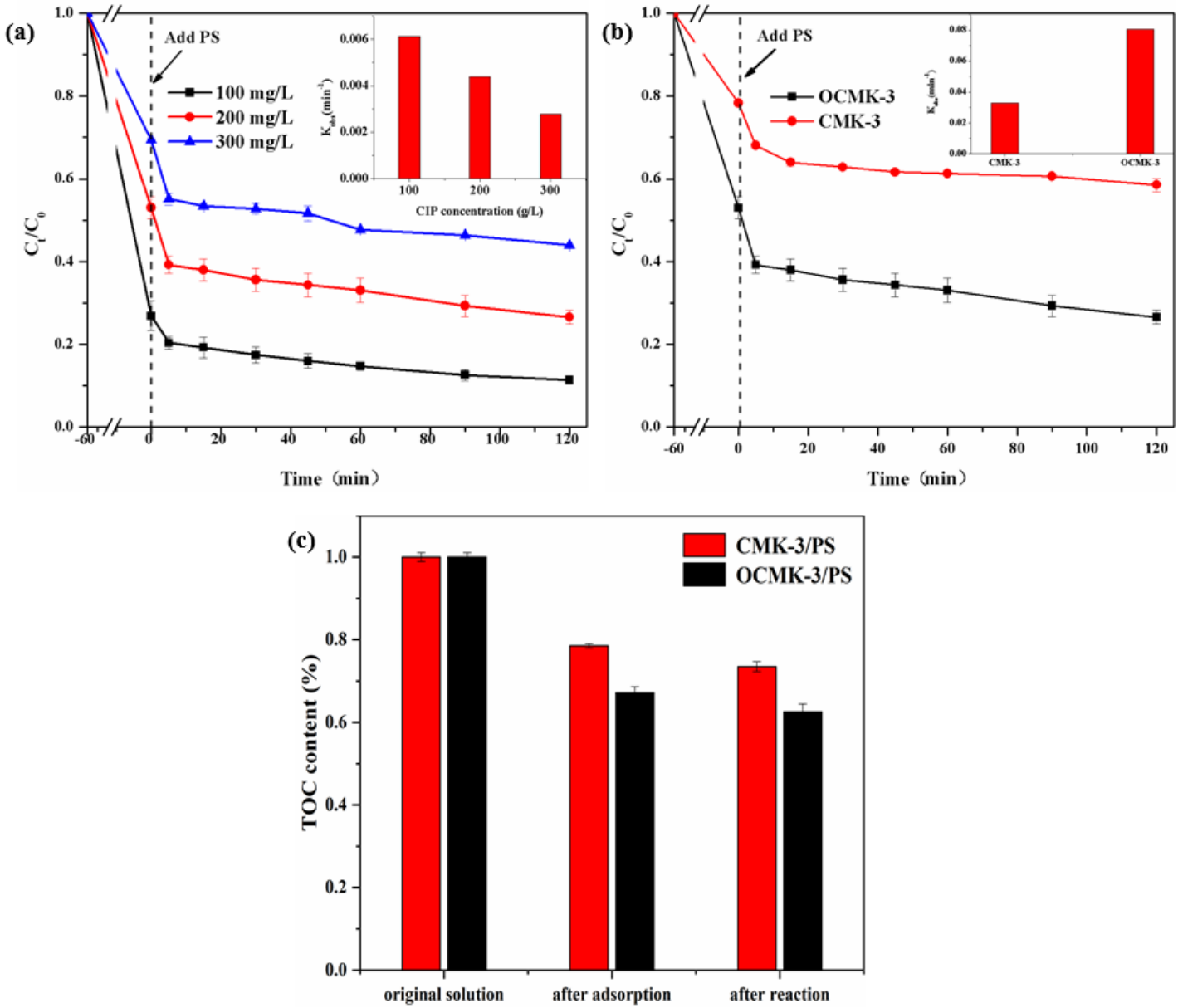

Figure 6

(a) Effect of initial concentration of CIP on its removal; (b) CIP removal on CMK-3 and OCMK-3 ([CIP=200mg/L]); (c) TOC removal rate in different systems ([CIP=200mg/L]). Insets are the corresponding changes of pseudo-first-order rate constant. Conditions: [CMK-3/OCMK-3] = 0.2 g/L, [PS] = 8 mM, [Temp] = 25°C.

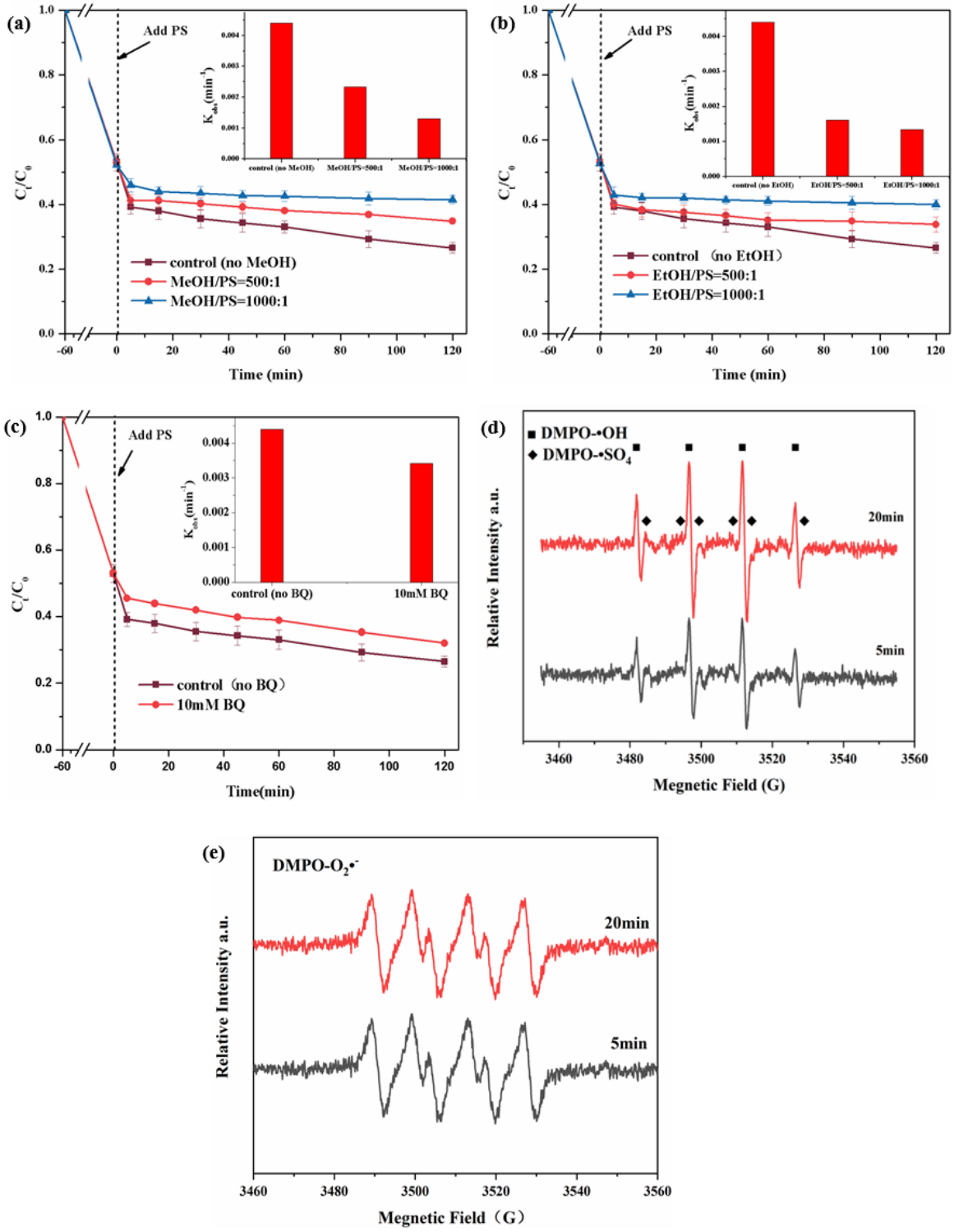

Figure 7

Effects of (a) MeOH and (b) Ethanol on CIP remove at different molar ratio with PS; (c) Effects of BQ (10 mM) on CIP removal; (d–e) EPR spectra of PS activation by OCMK-3. Conditions: [CIP]=200mg/L, [PS] = 8mM, [OCMK-3] = 0.2 g/L, [Temp] = 25°C.

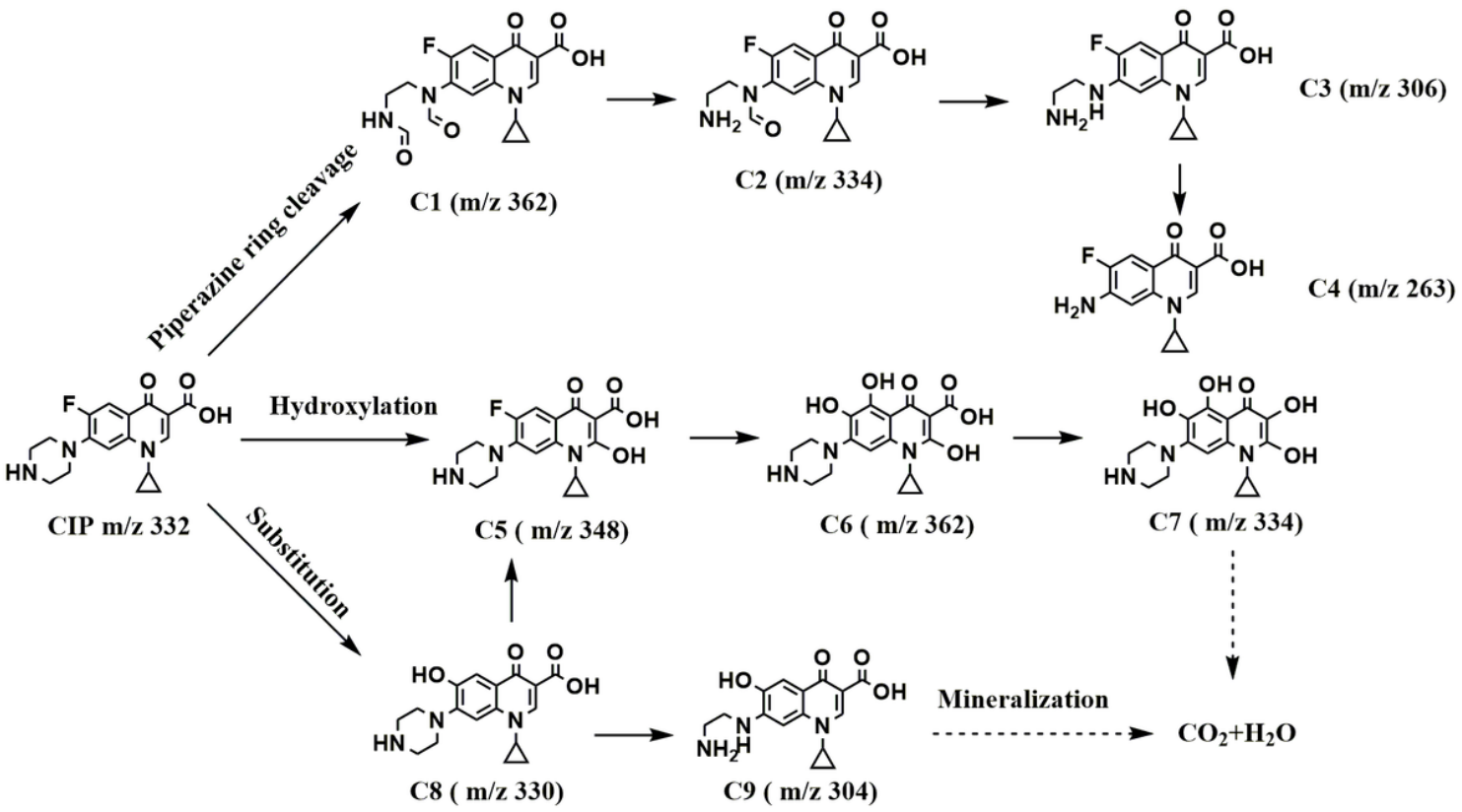

Figure 8

Possible degradation pathway of CIP in the OCMK-3/ PS system.

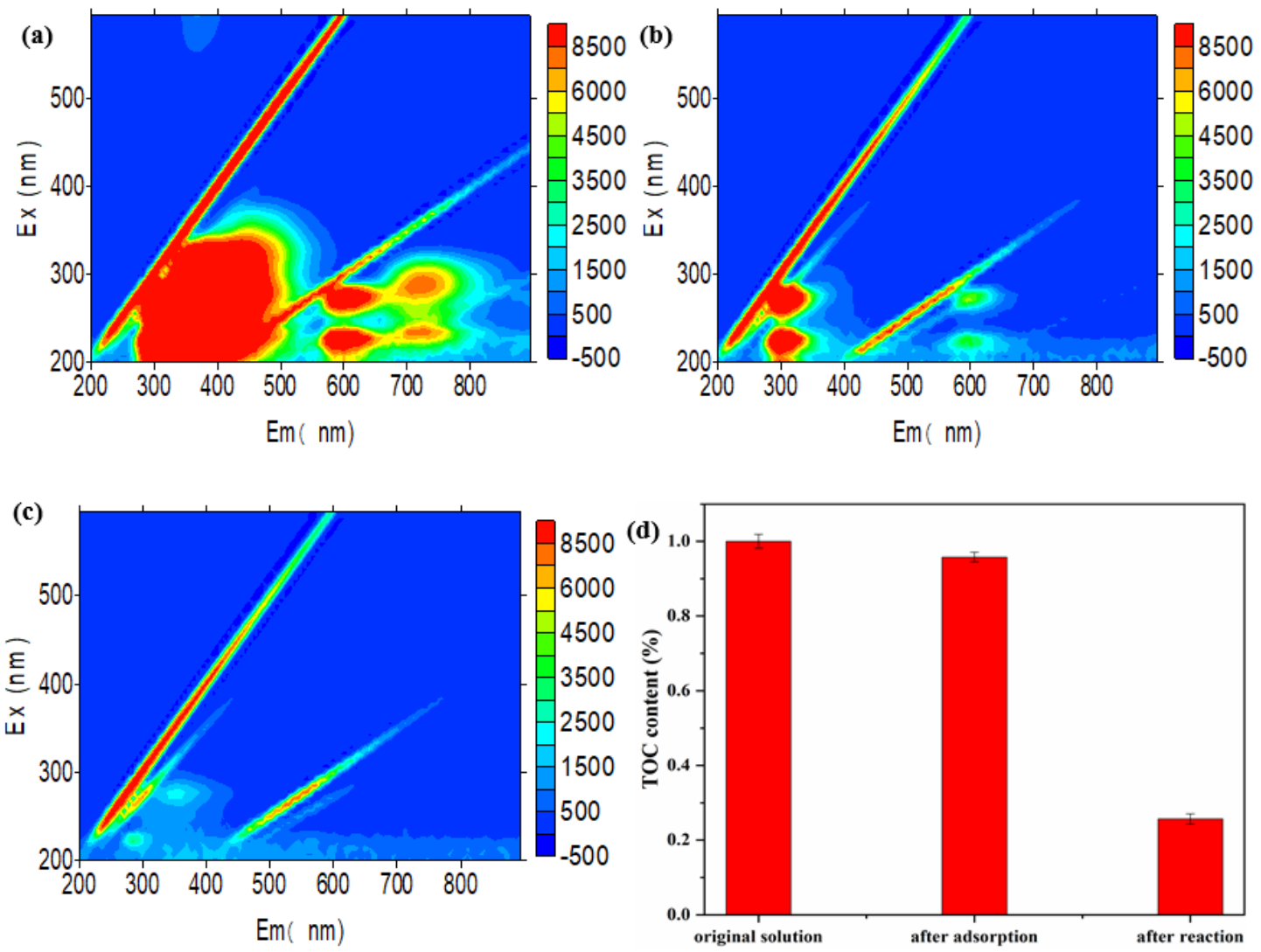

Figure 9

Three-dimensional excitation and emission matrix (3D-EEM) fluorescence spectroscopy of (a) the original water sample, (b) the sample after adsorption by OCMK-3 for 1 h and (c) the sample after reaction with OCMK-3/PS for 2 h; (d) The TOC changes of the real water sample. Conditions: [PS] =8mM, [OCMK-3] = 0.2 g/L, [Temp] = 25°C.

Supplementary Files

This is a list of supplementary files associated with this preprint. Click to download.

- Scheme1.png
- supplemetarymaterials.docx